Acta Mech 227, 1005–1023 (2016)
DOI 10.1007/s00707-015-1495-z

ORIGINAL PAPER

Yueqiu Li · Peijun Wei · Yahong Zhou

Band gaps of elastic waves in 1-D phononic crystal with dipolar gradient elasticity

Received: 9 June 2015 / Revised: 24 August 2015 / Published online: 15 December 2015

Abstract The dispersive relations of Bloch waves in the periodic laminated structure formed by periodically repeating two different gradient elastic solids are studied in this paper. First, the various wave modes in the gradient elastic solid, which are different from those in the classical elastic solid, are formulated. Apart from the dispersive P wave and SV wave, there are two evanescent waves, which become the P type and S type surface waves at the interface of two different gradient elastic solids. Next, the continuity conditions of the displacement vector, the normal derivative of the displacement vector and the monopolar and dipolar tractions across the interface between two different gradient elastic solids are used to derive the transfer matrix of the state vector in a typical single cell. At last, the Bloch theorem of Bloch waves in the periodical structure is used to give the dispersive equation. The in-plane Bloch waves and the anti-plane Bloch waves are both considered in the present work. The oblique propagation situation and the normal propagation situation are also considered, respectively. The numerical results are obtained by solving the dispersive equation. The influences of two microstructure parameters of the gradient elastic solid and the microstructure parameter ratio of two different gradient elastic solids on the dispersive relation are discussed based on the numerical results.

1 Introduction

Since the conception of "phononic crystal" was proposed by [17], the propagation behavior of elastic waves in the phononic crystal has attracted wide attention [18,23,27,28,30,36]. The so called phononic crystal is an artificial composite material with designable periodical structure, which can control the propagation of elastic waves. The one-dimensional phononic crystal is the periodical laminated structure. The propagation of elastic waves through a one-dimensional phononic crystal may lead to the appearance of Bloch waves with a periodically modulated amplitude and exhibits the band gap property which means the material is of frequency selectivity for the elastic waves propagating through it. Apart from the periodic lattice, the material properties of the components material are important for creating the band gap. Therefore, the reserved on the phononic crystal gradually is extended to or more wide type of material from the classical isotropic elastic solids. Zhan and Wei [39,40] studied band gaps of a 2D phononic crystal with orthotropic cylindrical fillers and a 3D phononic crystal with orthotropic spherical inclusions embedded in the isotropic host. Zhao and Wei [37,38] studied the one-dimensional crystal phononic and the two-dimensional phononic crystal with viscoelastic host. The influences of viscoelastic properties on the dispersive relation and band gap are investigated based on the complex moduli. Wang et al. [34,35] studied the propagation of elastic waves in phononic crystals consisting of

Y. Li · P. Wei (✉) · Y. Zhou
Department of Applied Mechanics, University of Sciences and Technology Beijing, Beijing 100083, China
E-mail: weipj@ustb.edu.cn

P. Wei
State Key Laboratory of Nonlinear Mechanics (LNM), Chinese Academy of Science, Beijing, China

piezoelectric or piezomagnetic elastic solids. The influences of the mechanical and electrical coupling effects on the dispersive relation and band gaps are considered. Pang et al [27] studied the propagation behaviors of elastic waves in 1D piezoelectric/piezomagnetic phononic crystals with line defects by the stiffness matrix method. Lan and Wei [19,20] further studied the dispersive characteristics of elastic waves propagating through a laminated piezoelectric phononic crystal with mechanically imperfect interfaces and the gradient interlayer. These above-mentioned investigations are basically applicable to the Bloch waves with long wavelength. Because the wavelength of Bloch waves is much larger than the characteristic length of the microstructure in the macroscopical homogeneous medium, the microstructure effects can be ignored.

With the development of micro- and nano-phononic crystals, the propagation behavior of Bloch waves with short wavelength gets attention gradually. When the wavelength of Bloch waves is comparable to the characteristic length of the microstructure, the microstructure effects cannot be ignored anymore. In order to take the microstructure effects into consideration, the classical elasticity theory should be replaced by the advanced elasticity theory with consideration of microstructure effects, for example the couple stress theory [24,31], the non-local theory [7], the micropolar and micromorphic theory [4,5]. Parfitt and Eringen [26] studied the propagation of an elastic wave in the micropolar solid. It is found that there are four kinds of dispersive bulk waves, which are different from those in the classical elastic solid. Tomar and Gogna [32] further studied the reflection and refraction of a wave at an interface between two micropolar elastic solids at welded contact. Tomar and Monika [33] studied the reflection and transmission of waves from a plane interface between two microstretch solid half-spaces. Georgiadis et al. [11] studied the propagation behavior of the Rayleigh wave along the surface of a half-space of a microstructure solid characterized by dipolar gradient elasticity (or strain gradient elasticity of grade two). Their investigation showed that the Rayleigh wave is dispersive, which is consistent with the experimental observation. This remedies the shortcoming of the classical theory of elasticity which predicts that a Rayleigh wave is not dispersive at any frequency. Gourgiotis et al. [12] further studied the reflection of elastic waves at the free boundary of the microstructured solids governed by the dipolar gradient elasticity. This theory was actually introduced by Green and Rivlin [8], Green [9], and Mindlin [25] in an effort to model the mechanical response of materials with microstructure. The term "dipolar gradient elasticity" was first used when [10] studied the crack problem in the microstructure solids. The theory begins with the very general concept of a continuum containing elements or particles (called macromedia), and such a macro-particle is further viewed as a collection of smaller subparticles (called micro-media). Each particle of the continuum is endowed with an internal displacement field, which is expanded as a power series in internal coordinate variables. Within the above context, the lowest order theory (dipolar or grade-two theory) is the one obtained by retaining only the linear term. Since the strain energy is dependent on the strain gradients in the theory, the new material constants imply the presence of characteristic lengths in the material behavior, and thus, the size effects can be incorporated into the constitutive equation. Recently, [13] also studied the existence of torsional and SH surface waves in a half-space of a homogeneous and isotropic material and in the context of the complete Toupin–Mindlin theory of gradient elasticity where five additional material constants having dimensions of [force] are introduced. Li and Wei [21] further studied the reflection and transmission of plane waves at the interface between two different gradient elastic half-spaces. Their investigation shows that the microstructure effects have evident influences on the propagation behavior of the elastic waves when the wavelength of the elastic waves is comparable to the characteristic length of the microstructure.

In this paper, the one-dimensional phononic crystal consisting of two different gradient elastic solids which repeat periodically is studied. The microstructure effects are embodied by two microstructure constants in the present gradient elastic model. One is related to the micro-strain gradient, while the other is related to the micro-inertia. The transfer matrix of a typical single cell is obtained by considering the dispersive bulk waves and the dispersive surface waves in the gradient elastic solids and the continuous conditions for the displacement vector, the normal derivative of the displacement vector, and the monopolar and dipolar tractions at the interface of two different gradient elastic solids. The dispersive equation is obtained by the application of the Bloch theorem and is solved numerically. The influences of the microstructure constants on the dispersive curves and the band gaps are discussed based on the numerical results obtained.

2 The theory of dipolar gradient elasticity

According to Mindlin's [25] elastic theory of solids with microstructure, the strain energy density can be expressed as

$$W = \frac{1}{2}c_{ijkl}\varepsilon_{ij}\varepsilon_{kl} + \frac{1}{2}b_{ijkl}\gamma_{ij}\gamma_{kl} + \frac{1}{2}a_{ijklmn}\chi_{ijk}\chi_{lmn} + d_{ijklm}\gamma_{ij}\chi_{klm} + f_{ijklm}\chi_{ijk}\varepsilon_{lm} + g_{ijkl}\gamma_{ij}\varepsilon_{kl} \quad (1)$$

where c_{ijkl}, b_{ijkl}, a_{ijklmn}, d_{ijklm}, f_{ijklm} and g_{ijkl} are the components of the elastic tensor. ε_{ij}, $\gamma_{ij}(=u_{j,i}-\psi_{ij})$ and $\chi_{ijk}(=\psi_{jk,i})$ are the macro-strain of macro-medium, relative deformation (the difference between the macro-displacement gradient and the micro-deformation), and the micro-deformation gradient (the macro-gradient of the micro-deformation), respectively. If the relative deformation is ignored, namely $\gamma_{ij} = 0$, then the strain energy density function is simplified as

$$W = \frac{1}{2}c_{ijkl}\varepsilon_{ij}\varepsilon_{kl} + \frac{1}{2}a_{ijklmn}\chi_{ijk}\chi_{lmn} + f_{ijklm}\chi_{ijk}\varepsilon_{lm}. \quad (2)$$

It means that the strain energy density is dependent on not only the strain but also the strain gradient. For an isotropic and centrosymmetric medium, the last term in Eq. (2) should be discarded. Here, a phenomenological simplified version is given as follows:

$$W = \left(\frac{1}{2}\lambda\varepsilon_{ii}\varepsilon_{jj} + \mu\varepsilon_{ij}\varepsilon_{ij}\right) + \left(\frac{1}{2}\lambda c\varepsilon_{ii,k}\varepsilon_{jj,k} + \mu c\varepsilon_{ij,k}\varepsilon_{ji,k}\right) \quad (3)$$

where the first term is the contribution from the strains; the second term is the contribution from the strain gradient. Define

$$\tau_{ij} = \frac{\partial W}{\partial \varepsilon_{ij}} = \lambda\delta_{ij}\varepsilon_{pp} + 2\mu\varepsilon_{ij}, \quad (4.1)$$

$$\mu_{kij} = \frac{\partial W}{\partial \chi_{kij}} = c\left(\lambda\delta_{ij}\varepsilon_{pp} + 2\mu\varepsilon_{ij}\right)_{,k} \quad (4.2)$$

where λ and μ are the classical Lamé constants; c is a microstructure parameter with dimension of m^2; τ_{ij} is the Cauchy stress or monopolar stress; and μ_{ijk} is the dipolar stress with the dimensions of Nm^{-1}. The monopolar stress and the dipolar stress are corresponding with the notion of monopolar force and the dipolar force, respectively. The monopolar forces are the classical forces, and the dipolar forces are the anti-parallel forces acting between the micro-media contained in the continuum with microstructure. It is noted that there is a microstructure parameter c involved in the constitutive equations. Therefore, the microstructure effects can be captured to a certain extent.

The kinetic energy density includes two terms. One involves the velocity, and the other term involves the velocity gradient,

$$T = \frac{1}{2}\rho\dot{u}_j\dot{u}_j + \frac{1}{6}\rho d^2\dot{u}_{k,j}\dot{u}_{k,j}, \quad (5)$$

where ρ is the mass density and d is the characteristic length of the microstructure.

The work done by the external forces is

$$W_1 = \int_V F_k u_k \mathrm{d}V + \int_S P_k u_k \mathrm{d}S + \int_S R_k D u_k \mathrm{d}S, \quad (6)$$

where F_k is the body force, P_k is the monopolar traction, and R_k is the dipolar traction

Hamilton's variational principle requires

$$\delta\int_{t_0}^{t_1}\int_V (T - W)\mathrm{d}V\mathrm{d}t + \int_{t_0}^{t_1}\int_S \delta W_1 \mathrm{d}S\mathrm{d}t = 0, \quad (7)$$

which leads to the motion equation and the boundary condition

$$\left(\tau_{jk} - \mu_{ijk,i}\right)_{,j} + F_k = \rho\ddot{u}_k - \frac{\rho d^2}{3}\ddot{u}_{k,jj}, \text{ in V}, \quad (8)$$

$$P_k = n_j\left(\tau_{jk} - \mu_{ijk,i}\right) - D_j\left(n_i\mu_{ijk}\right) + (D_l n_l)\, n_i n_j \mu_{ijk} + \frac{\rho d^2}{3} n_j \ddot{u}_{k,j}, \text{ on surface} \quad (9.1)$$

$$R_k = n_i n_j \mu_{ijk}, \text{ on surface} \quad (9.2)$$

where n_j is the normal of the boundary of the solid. $D_j = (\delta_{jl} - n_j n_l)\partial_l$, $D = n_l\partial_l$.

3 The elastic wave in the dipolar gradient elastic solid

Inserting Eq. (4) into Eq. (8) and ignoring the volume force lead to the equation of motion in terms of the displacement,

$$\left(1-c\nabla^2\right)\left[(\lambda+\mu)\nabla\nabla\cdot\mathbf{u}+\mu\nabla^2\mathbf{u}\right]=\rho\ddot{\mathbf{u}}-\frac{\rho d^2}{3}\nabla^2\ddot{\mathbf{u}}, \tag{10}$$

where ∇^2 is the Laplace operator. Equation (10) reduces to the Navier equation in the classical elastic theory when the microstructure parameters c and d are taken to be zero. It is noted that the microstructure parameters c and d appear in the motion equation. It means that the microstructure effects will influence the wave propagation modes in the solid. Next, let us discuss the elastic wave propagation in the dipolar gradient elastic solid. Supposing the propagation plane is oxy, we will discuss the in-plane wave and the anti- plane wave, respectively.

(i) In the case of an anti-plane wave, the displacement vector $\mathbf{u}$ can be expressed as $\mathbf{u}=u_z(x,y)\,\mathbf{e}_z$. Accordingly, Eq. (10) reduces to

$$c\nabla^4u_z-\left(1-\frac{\omega^2d^2}{3V_s^2}\right)\nabla^2u_z-\frac{\omega^2}{V_s^2}u_z=0. \tag{11}$$

Equation (11) can be rewritten as

$$\left(\nabla^2+\sigma_{sh}^2\right)\left(\nabla^2-\tau_{sh}^2\right)u_z=0 \tag{12}$$

where

$$\sigma_{sh}=\left\{\frac{1}{2c}\left[\Delta_s-(1-m_s)\right]\right\}^{\frac{1}{2}},\quad \tau_{sh}=\left\{\frac{1}{2c}\left[\Delta_s+(1-m_s)\right]\right\}^{\frac{1}{2}},$$
$$m_s=\frac{\omega^2d^2}{3V_s^2},\quad V_s^2=\frac{\mu}{\rho},\quad \Delta_s=\left[(1-m_s)^2+\frac{4c\omega^2}{V_s^2}\right]^{\frac{1}{2}}.$$

Equation (12) means that there are two SH type waves. One of them has real wavenumber σ_{sh}; the other has imaginary wavenumber $i\tau_{sh}$. The real wavenumber signifies the propagating wave without attenuation, while the imaginary wavenumber signifies the attenuation nature. At the interface between two different dipolar gradient elastic solids, the solution of Eq. (12) can be expressed as

$$\begin{aligned}u_z=&H_1\exp\left[i\left(\xi y+\beta_{sh}x-\omega t\right)\right]+H_2\exp\left[i\left(\xi y-\beta_{sh}x-\omega t\right)\right]\\&+F_1\exp\left[-\gamma_{sh}x+i\left(\xi y-\omega t\right)\right]+F_2\exp\left[+\gamma_{sh}x+i\left(\xi y-\omega t\right)\right]\end{aligned} \tag{13}$$

where ξ is the apparent wavenumber along the y-axis, $\beta_{sh}^2=\sigma_{sh}^2-\xi^2$ and $\gamma_{sh}^2(=\tau_{sh}^2+\xi^2)$. Equation (13) means that there are one SH type bulk wave and one SH type surface wave induced at the interface. β_{sh} is the projection of the wave vector of the bulk wave on y-axis. H_1 and H_2 are the amplitudes of two bulk waves toward and away the interface (also called as the forward and backward SH waves); γ_{sh} is the attenuation coefficient of surface waves. F_1 and F_2 are the amplitudes of two surface waves (called SSH waves), which are located at two sides of the interface but propagate along y-axis. It is noted that both SH bulk wave and SH type surface wave are dispersive, and the dispersive relations of them can be expressed as

$$\omega^2=\sigma_{sh}^2V_{sh}^2(1+c\sigma_{sh}^2)\left(1+\frac{d^2}{3}\sigma_{sh}^2\right)^{-1}, \tag{14.1}$$

$$\omega^2=\tau_{sh}^2V_s^2(1-c\tau_{sh}^2)\left(\frac{d^2}{3}\tau_{sh}^2-1\right)^{-1}. \tag{14.2}$$

(ii) In the case of an in-plane wave, the application of Helmholtz vector decomposition,

$$\mathbf{u}(x,y)=u_x(x,y)\,\mathbf{e}_x+u_y(x,y)\,\mathbf{e}_y=\nabla\varphi(x,y)+\nabla\times\psi(x,y)\mathbf{e}_z, \tag{15}$$

leads to

$$\left(\nabla^2+\sigma_p^2\right)\left(\nabla^2-\tau_p^2\right)\varphi=0, \tag{16.1}$$

$$\left(\nabla^2+\sigma_s^2\right)\left(\nabla^2-\tau_s^2\right)\psi=0. \tag{16.2}$$

Equation (16) means that there are two traveling waves of wavenumber σ_p and σ_s and two evanescent waves with imaginary wavenumber or attenuation factor τ_p and τ_s. At the interface between two different dipolar gradient elastic solids, the solution of Eq. (16) can be expressed as

$$\varphi(x,y,t)=\tilde{\varphi}(x)\exp\left[i\left(\xi y-\omega t\right)\right], \tag{17.1}$$

$$\psi(x,y,t)=\tilde{\psi}(x)\exp\left[i\left(\xi y-\omega t\right)\right]. \tag{17.2}$$

Inserting Eq. (17) into Eq. (16) leads to

$$\left(\frac{d^2}{dx^2}+\beta_p^2\right)\left(\frac{d^2}{dx^2}-\gamma_p^2\right)\tilde{\varphi}(x)=0, \tag{18.1}$$

$$\left(\frac{d^2}{dx^2}+\beta_s^2\right)\left(\frac{d^2}{dx^2}-\gamma_s^2\right)\tilde{\psi}(x)=0 \tag{18.2}$$

where

$$\beta_p^2=\sigma_p^2-\xi^2,\quad \gamma_p^2=\tau_p^2+\xi^2,\quad \beta_s^2=\sigma_s^2-\xi^2,\quad \gamma_s^2=\tau_s^2+\xi^2,$$

$$\sigma_p=\left\{\frac{1}{2c}\left[\Delta_p-\left(1-m_p\right)\right]\right\}^{\frac{1}{2}},\quad \tau_p=\left\{\frac{1}{2c}\left[\Delta_p+\left(1-m_p\right)\right]\right\}^{\frac{1}{2}},$$

$$\sigma_s=\left\{\frac{1}{2c}\left[\Delta_s-(1-m_s)\right]\right\}^{\frac{1}{2}},\quad \tau_s=\left\{\frac{1}{2c}\left[\Delta_s+(1-m_s)\right]\right\}^{\frac{1}{2}},$$

$$m_p=\frac{\omega^2d^2}{3V_p^2},\quad m_s=\frac{\omega^2d^2}{3V_s^2},\quad \Delta_p=\left[\left(1-m_p\right)^2+\frac{4c\omega^2}{V_p^2}\right]^{\frac{1}{2}},\ \Delta_s=\left[(1-m_s)+\frac{4c\omega^2}{V_s^2}\right]^{\frac{1}{2}},$$

$$V_p^2=\frac{\lambda+2\mu}{\rho},\quad V_s^2=\frac{\mu}{\rho}.$$

Inserting the solution of $\tilde{\varphi}(x)$ and $\tilde{\psi}(x)$ into Eq. (17), we obtain

$$\begin{aligned}\varphi=&A_1\exp\left[i\left(\xi y+\beta_p x-\omega t\right)\right]+A_2\exp\left[i\left(\xi y-\beta_p x-\omega t\right)\right]\\&+C_1\exp\left[-\gamma_p x+i\left(\xi y-\omega t\right)\right]+C_2\exp\left[+\gamma_p x+i\left(\xi y-\omega t\right)\right],\end{aligned} \tag{19.1}$$

$$\begin{aligned}\psi=&B_1\exp\left[i\left(\xi y+\beta_s x-\omega t\right)\right]+B_2\exp\left[i\left(\xi y-\beta_s x-\omega t\right)\right]\\&+D_1\exp\left[-\gamma_s x+i\left(\xi y-\omega t\right)\right]+D_2\exp\left[+\gamma_s x+i\left(\xi y-\omega t\right)\right]\end{aligned} \tag{19.2}$$

where A_i, B_i, C_i and D_i are the amplitudes of various waves. Equation (19) means that there is a traveling wave (P wave) of wavenumber σ_p and a traveling wave (SV wave) of wavenumber σ_s, respectively. In addition, there is a P type surface wave with imaginary wavenumber $i\tau_p$ and an S type surface wave with imaginary wavenumber $i\tau_s$. It is noted that not only P wave and SV wave but also the P type surface and the S type surface waves are dispersive, and the dispersive relations of them can be expressed as

$$\omega^2=\sigma_p^2V_p^2(1+c\sigma_p^2)\left(1+\frac{d^2}{3}\sigma_p^2\right)^{-1}, \tag{20.1}$$

$$\omega^2=\sigma_s^2V_s^2(1+c\sigma_s^2)\left(1+\frac{d^2}{3}\sigma_s^2\right)^{-1}, \tag{20.2}$$

$$\omega^2=\tau_p^2V_p^2(1-c\tau_p^2)\left(\frac{d^2}{3}\tau_p^2-1\right)^{-1}, \tag{20.3}$$

$$\omega^2=\tau_s^2V_s^2(1-c\tau_s^2)\left(\frac{d^2}{3}\tau_s^2-1\right)^{-1}. \tag{20.4}$$

We also note some special cases. (a) When $\beta_p^2 = 0$ and $\beta_s^2 = 0$, this means that both P wave and SV wave propagate along the direction parallel to the interface. (b) When $\beta_p^2 < 0$ and $\beta_s^2 < 0$, this means all bulk waves disappear. (c) When $\beta_p^2 > 0$ and $\beta_s^2 > 0$, this means the bulk wave and the surface waves coexist. The third case is our main concern in this paper. Recall that $\beta_p^2 = \sigma_p^2 - \xi^2$, $\beta_s^2 = \sigma_s^2 - \xi^2$, $\sigma_p = \omega/v_p^g$, $\sigma_s = \omega/v_s^g$. For a given apparent wavenumber ξ, there is a cutoff frequency, namely

$$\omega_{cr}^p = \xi v_p^g, \tag{21.1}$$

$$\omega_{cr}^s = \xi v_s^g \tag{21.2}$$

for P wave and SV wave, respectively. Wherein $v_p^g(=\omega/\sigma_p)$ and $v_s^g(=\omega/\sigma_s)$ are the phase speeds of P wave and SV wave, respectively.

4 Dispersion relation of a Bloch wave in an oblique propagation situation

Consider a typical single cell in the one-dimensional laminated structure of gradient elastic solids. The single cell is composed of two different gradient elastic solids with thickness of a_1 and a_2, see Fig. 1. The wave propagation plane is assumed to be oxy, where the x-axis is along the normal direction of the laminated structure and the y-axis is along the interface.

4.1 Dispersion relation of an anti-plane Bloch wave

In the anti-plane situation, the monopolar traction and the dipolar traction in Eqs. (9) and (10) reduce to

$$P_z = \mu\left[(1-a_s)\,u_{z,x} - c\left(u_{z,xxx} + 2u_{z,xyy}\right)\right], \tag{22.1}$$

$$R_z = \mu c u_{z,xx}. \tag{22.2}$$

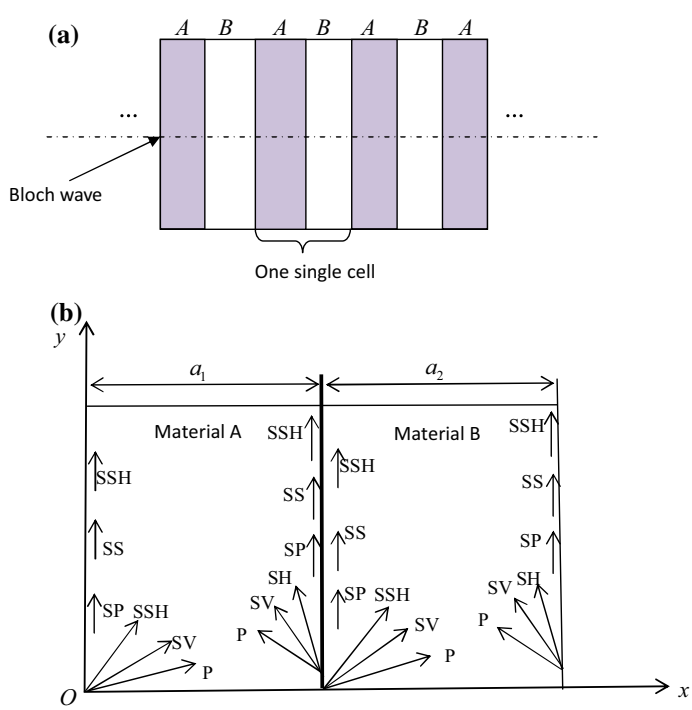

Fig. 1 The sketch of a typical single cell in the periodic laminated structure of gradient elastic solids. **a** The periodic laminated structure of gradient elastic solids; **b** the anti-plane and in-plane waves in a typical single cell in oblique propagation situation

The displacement field in any layer in a typical single cell is formed by the forward and the backward SH bulk waves plus two surface waves propagating along the interface, which are expressed in Eq. (13). Define the state vector

$$\mathbf{V} = \left[u_z, u_{z,x}, P_z, R_z\right]^T. \tag{23}$$

Then, the state vector at the left and right boundaries of a layer can be expressed as

$$\mathbf{V}^L = P\left[H_1, H_2, F_1, F_2\right]^T \exp\left[i\left(\xi y - \omega t\right)\right], \tag{24.1}$$
$$\mathbf{V}^R = PG\left[H_1, H_2, F_1, F_2\right]^T \exp\left[i\left(\xi y - \omega t\right)\right] \tag{24.2}$$

where $\mathbf{V}^L = \left[u_z^L, u_{z,x}^L, P_z^L, R_z^L\right]^T$ and $\mathbf{V}^R = \left[u_z^R, u_{z,x}^R, P_z^R, R_z^R\right]^T$. G is a diagonal matrix, namely G=diag(exp($i\beta_{si}a_i$), exp($-i\beta_{si}a_i$), exp($-\gamma_{si}a_i$), exp($\gamma_{si}a_i$)). Let the transfer matrix T relate the state vectors at the left and right boundaries of a layer by

$$\mathbf{V}^R = T\mathbf{V}^L. \tag{25}$$

Then,

$$T = PGP^{-1}. \tag{26}$$

The transfer matrix T is determined by the material constants, the thickness of this layer and the various wave modes in this layer. The explicit expressions of transfer matrix T are given in "Appendix 1". Let

$$\mathbf{V}_A^R = T_A\mathbf{V}_A^L, \tag{27.1}$$
$$\mathbf{V}_B^R = T_B\mathbf{V}_B^L \tag{27.2}$$

where T_A and T_B are the transfer matrix of layer A and layer B, respectively. For the perfect interface situation, the state vector is continuous across the interface between layer A and layer B, namely

$$\mathbf{V}_A^R = \mathbf{V}_B^L. \tag{28}$$

This interface condition leads to

$$\mathbf{V}_B^R = T_B T_A \mathbf{V}_A^L. \tag{29}$$

The Bloch theorem for the wave propagation in the periodic structure can be expressed as

$$\mathbf{V}_B^R = \exp(ik_x a)\mathbf{V}_A^L \tag{30}$$

where $a(=a_1 + a_2)$ is the thickness of a typical single cell. k_x is the wavenumber of a Bloch SH wave in the periodic laminated structure.

Inserting Eq. (29) into Eq. (30) leads to

$$\left[\mathbf{T}_B\mathbf{T}_A - \mathbf{I}\cdot\exp(ik_x a)\right]\mathbf{V}_A^L = 0. \tag{31}$$

The existence of non-trivial solution requires

$$\left|\mathbf{T}_B\mathbf{T}_A - \mathbf{I}\exp(ik_x a)\right| = f(\omega, \xi, k_x) = 0. \tag{32}$$

Equation (32) is the dispersive relation of a Bloch SH wave.

4.2 Dispersion relation of an in-plane Bloch wave

In the in-plane wave situation, the monopolar traction and the dipolar traction in Eqs. (9) reduce to

$$\begin{aligned} P_x &= \left(1 - c\nabla^2\right)\left[\lambda\nabla^2\varphi + 2\mu\left(\varphi_{,xx} + \psi_{,xy}\right)\right] \\ &\quad - c\mu\left[\nabla^2\psi + 2\left(\varphi_{,xy} - \psi_{,xx}\right)\right]_{,xy} - \frac{\rho d^2\omega^2}{3}\left(\varphi_{,xx} + \psi_{,xy}\right) \qquad (33.1) \\ P_y &= \left(1 - c\nabla^2\right)\left[\mu\nabla^2\psi + 2\mu\left(\varphi_{,xy} - \psi_{,xx}\right)\right] \\ &\quad - c\left[\lambda\nabla^2\varphi + 2\mu\left(\varphi_{,yy} - \psi_{,xy}\right)\right]_{,xy} - \frac{\rho d^2\omega^2}{3}\left(\varphi_{,xy} - \psi_{,xx}\right), \qquad (33.2) \\ R_x &= c\left[\lambda\nabla^2\varphi + 2\mu\left(\varphi_{,xx} + \psi_{,xy}\right)\right]_{,x}, \qquad (33.3) \\ R_y &= c\left[\mu\nabla^2\psi + 2\mu\left(\varphi_{,xy} - \psi_{,xx}\right)\right]_{,x}. \qquad (33.4) \end{aligned}$$

The displacement field in any layer in a typical single cell is formed by the forward and the backward P and SV bulk waves plus two P type surface waves and two S type surface waves propagating along the interface, which are expressed in Eq. (19). Define the state vector

$$\mathbf{V} = \left[u_x, u_y, u_{x,x}, u_{y,x}, P_x, P_y, R_x, R_y\right]^T. \qquad (34)$$

Then, the state vector at the left and right boundaries of a layer can be expressed as

$$\begin{aligned} \mathbf{V}^L &= P\left[A_1, A_2, C_1, C_2, B_1, B_2, D_1, D_2\right]^T \exp\left[i\left(\xi y - \omega t\right)\right], \qquad (35.1) \\ \mathbf{V}^R &= Q\left[A_1, A_2, C_1, C_2, B_1, B_2, D_1, D_2\right]^T \exp\left[i\left(\xi y - \omega t\right)\right] \qquad (35.2) \end{aligned}$$

where G is a diagonal matrix, namely G=diag($\exp(i\beta_{pi}a_i)$, $\exp(-i\beta_{pi}a_i)$, $\exp(-i\gamma_{pi}a_i)$, $\exp(i\gamma_{pi}a_i)$, $\exp(i\beta_{si}a_i)$, $\exp(-i\beta_{si}a_i)$, $\exp(-i\gamma_{si}a_i)$, $\exp(i\gamma_{si}a_i)$).

Let

$$\mathbf{V}^R = T\mathbf{V}^L. \qquad (36)$$

Then, the transfer matrix T can be obtained by

$$T = PGP^{-1}. \qquad (37)$$

The explicit expressions of T are given in "Appendix 2". Further, by application of the continuous condition of the state vector across the interface between two gradient elastic solids, the state vector at the left and right boundaries of a typical single cell can be related by

$$\mathbf{V}_B^R = T_B T_A \mathbf{V}_A^L \qquad (38)$$

where T_A and T_B is the transfer matrix of layer A and layer B, respectively, namely $\mathbf{V}_A^R = T_A\mathbf{V}_A^L, \mathbf{V}_B^R = T_B\mathbf{V}_B^L$. Similar as in the anti-plane situation, the application of the Bloch theorem leads to the dispersive relation of an in-plane Bloch wave,

$$\left|\mathbf{T}_B\mathbf{T}_A - \mathbf{I}\exp(ik_x a)\right| = f(\omega, \xi, k_x) = 0. \qquad (39)$$

Although Eq. (39) has the same form like Eq. (32), solving Eq. (39) is much more complicated than solving Eq. (32). This can be understandable when we recall that the transfer matrices T_A and T_B are of 8×8 orders in in-plane Bloch wave situation and are of 4×4 order in anti-plane Bloch wave situation.

5 Dispersion relation of a Bloch wave in normal propagation situation

In the normal propagation situation, the P wave, SV wave and SH wave are decoupled from each other. The dispersive equations of Bloch SH wave, Bloch P wave and Bloch SV wave have the same form, namely

$$|\mathbf{T}_B\mathbf{T}_A - \mathbf{I}\exp(ika)| = f(\omega, k) = 0. \tag{40}$$

The displacement field of a Bloch SH wave and the corresponding monopolar traction and the dipolar traction are

$$\begin{aligned} u_z &= H_1 \exp\left[i\left(\sigma_{sh}x - \omega t\right)\right] + H_2 \exp\left[i\left(-\sigma_{sh}x - \omega t\right)\right] \\ &\quad + F_1 \exp\left(-\tau_{sh}x - i\omega t\right) + F_2 \exp\left(+\tau_{sh}x - i\omega t\right), \end{aligned} \tag{41.1}$$

$$\begin{aligned} u_{z,x} &= i\sigma_{sh}H_1 \exp\left[i\left(\sigma_{sh}x - \omega t\right)\right] - i\sigma_{sh}H_2 \exp\left[i\left(-\sigma_{sh}x - \omega t\right)\right] \\ &\quad - \tau_{sh}F_1 \exp\left(-\tau_{sh}x - i\omega t\right) + \tau_{sh}F_2 \exp\left(\tau_{sh}x - i\omega t\right), \end{aligned} \tag{41.2}$$

$$P_z = \mu\left[\left(1 - a_s\right)u_{z,x} - cu_{z,xxx}\right], \tag{41.3}$$

$$R_z = \mu c u_{z,xx}. \tag{41.4}$$

The displacement field of a Bloch P wave and the corresponding monopolar traction and the dipolar traction are

$$\begin{aligned} u_x &= i\sigma_p A_1 \exp\left[i\left(\sigma_p x - \omega t\right)\right] - i\sigma_p A_2 \exp\left[i\left(-\sigma_p x - \omega t\right)\right] \\ &\quad - \tau_p C_1 \exp\left(-\tau_p x - i\omega t\right) + \tau_p C_2 \exp\left(+\tau_p x - i\omega t\right), \end{aligned} \tag{42.1}$$

$$\begin{aligned} u_{x,x} &= -\sigma_p^2 A_1 \exp\left[i\left(\sigma_p x - \omega t\right)\right] - \sigma_p^2 A_2 \exp\left[i\left(-\sigma_p x - \omega t\right)\right] \\ &\quad + \tau_p^2 C_1 \exp\left(-\tau_p x - i\omega t\right) + \tau_p^2 C_2 \exp\left(+\tau_p x - i\omega t\right), \end{aligned} \tag{42.2}$$

$$P_x = (\lambda + 2\mu)\left[\left(1 - c\nabla^2\right) - a_p\right]u_{x,x}, \tag{42.3}$$

$$R_x = c\left(\lambda + 2\mu\right)u_{x,xx}. \tag{42.4}$$

The displacement field of a Bloch SV wave and the corresponding monopolar traction and the dipolar traction are

$$\begin{aligned} u_y &= i\sigma_s B_1 \exp\left[i\left(\sigma_s x - \omega t\right)\right] - i\sigma_s B_2 \exp\left[i\left(-\sigma_s x - \omega t\right)\right] \\ &\quad - \tau_s D_1 \exp\left(-\tau_s x - i\omega t\right) + \tau_s D_2 \exp\left(\tau_s x - i\omega t\right), \end{aligned} \tag{43.1}$$

$$\begin{aligned} u_{y,x} &= -\sigma_s^2 B_1 \exp\left[i\left(\sigma_s x - \omega t\right)\right] - \sigma_s^2 B_2 \exp\left[i\left(-\sigma_s x - \omega t\right)\right] \\ &\quad + \tau_s^2 D_1 \exp\left(-\tau_s x - i\omega t\right) + \tau_s^2 D_2 \exp\left(\tau_s x - i\omega t\right), \end{aligned} \tag{43.2}$$

$$P_y = \mu\left[\left(1 - c\nabla^2\right) - a_s\right]u_{y,x}, \tag{43.3}$$

$$R_y = \mu c u_{y,xx}. \tag{43.4}$$

The explicit expressions of the transfer matrix $\mathbf{T}$ for the Bloch SH wave, Bloch P wave and Bloch SV wave are given, respectively, in "Appendix 3".

6 Numerical results and discussions

The dispersive relation (the dependence of wavenumber k_x upon the angular frequency ω) of Bloch waves in the periodical laminated structure is dependent upon (i) the thickness (a_1, a_2) of two gradient elastic solids; (ii) the material constants $(V_{pi}, V_{si}, \rho_i, c_i, d_i)$ of two gradient elastic solids; (iii) the apparent wavenumber (ξ) of Bloch waves (in the oblique propagation situation). In general, the dispersive equation can be written as

$$f\left(V_{p1}, V_{s1}, \rho_1, c_1, d_1, V_{p2}, V_{s2}, \rho_2, c_2, d_2, a_1, a_2, k_x, \xi, \omega\right) = 0. \tag{44}$$

Choose (a, ρ_1, ω) as the basic physical quantities; then, the non-dimensional form of the dispersive equation can be rewritten as

$$f\left(\frac{V_{p1}}{V_{s1}}, \frac{V_{s1}}{\omega a}, 1, \frac{\sqrt{c_1}}{a}, \frac{d_1}{a}, \frac{V_{p2}}{V_{p1}}, \frac{V_{s2}}{V_{s1}}, \frac{\rho_2}{\rho_1}, \frac{c_2}{c_1}, \frac{d_2}{d_1}, \frac{a_1}{a}, 1, k_x a, \xi a, 1\right) = 0. \tag{45}$$

In this numerical example, we mainly concern the influences of the following parameters: $\bar{c}_1 = \sqrt{c_1}/a$, $\bar{d}_1 = d_1/a$, $\bar{c} = c_1/c_2$, $\bar{d} = d_1/d_2$, $\bar{\xi} = \xi a$. Other parameters are given as follows: $V_{p1}/V_{s1} = 2.6621$, $V_{p2}/V_{p1} = 0.562$, $V_{s2}/V_{s1} = 0.5947$, $\rho_2/\rho_1 = 0.1573$, $a_1/a = 0.5$.

6.1 Anti-plane Bloch SH wave

For convenience of comparison, the dispersive curves of Bloch waves in the periodic laminated structure consisting of the classical elastic solids and the gradient elastic solids are given in Figs. 2 and 3, respectively. The horizontal axis denotes the normalized wavenumber (ka/π) of a Bloch SH wave in the first Brillouin zone. The vertical axis denotes the normalized angular frequency ($\omega a/2\pi v_m$, $v_m = a/(a_1/V_{sA} + a_2/V_{sB})$). $\bar{\xi}$(=ξa) denotes the normalized apparent wavenumber. $\bar{\xi} = 0$ stands for the normal propagation situation, while $\bar{\xi} \neq 0$ stands for the oblique propagation situation. The shadow zone denotes the band gap. From Figs. 2 and 3, it is observed that not only the dispersive curves but also the band gaps of the Bloch SH wave in the periodical laminated structure formed by the gradient elastic solids have evident deviation from those formed by the classical elastic solids. There are two kinds of dispersive wave modes (dispersive SH wave and SH type surface wave), which are different from the wave modes in the classical elastic solids (only non-dispersive SH bulk wave). This results in the deviation of dispersive curves and the band gaps. It is also observed that the dispersive curves shift toward the high frequency in the gradient elastic solids compared with the dispersive curves in the classical elastic solids. But the dispersive curves at low-frequency range shift more evident than

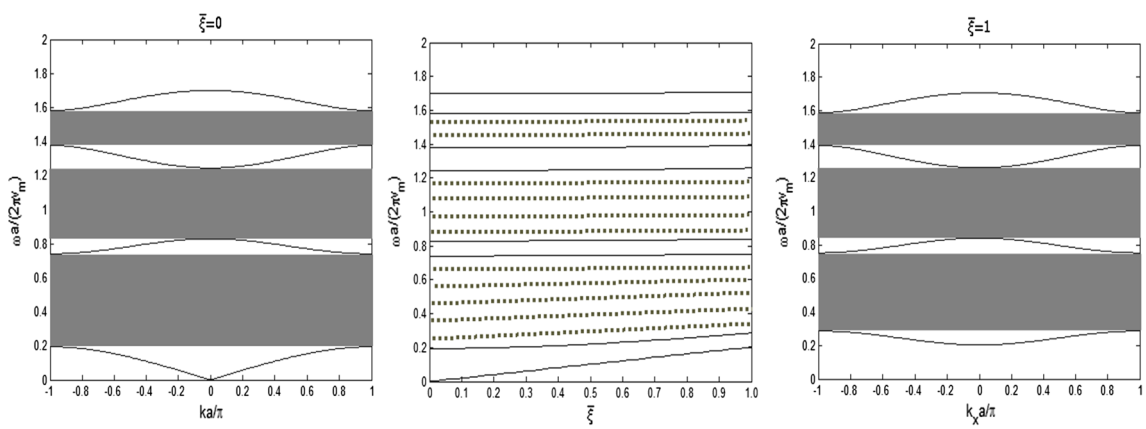

Fig. 2 The dispersive curves and band gaps of anti-plane Bloch waves in the periodic structure consisting of the classical elastic solids. *Left* in the normal propagation situation ($\bar{\xi} = 0$); *right* in the oblique propagation situation ($\bar{\xi} \neq 0$); *middle* the change of upper and lower band edge

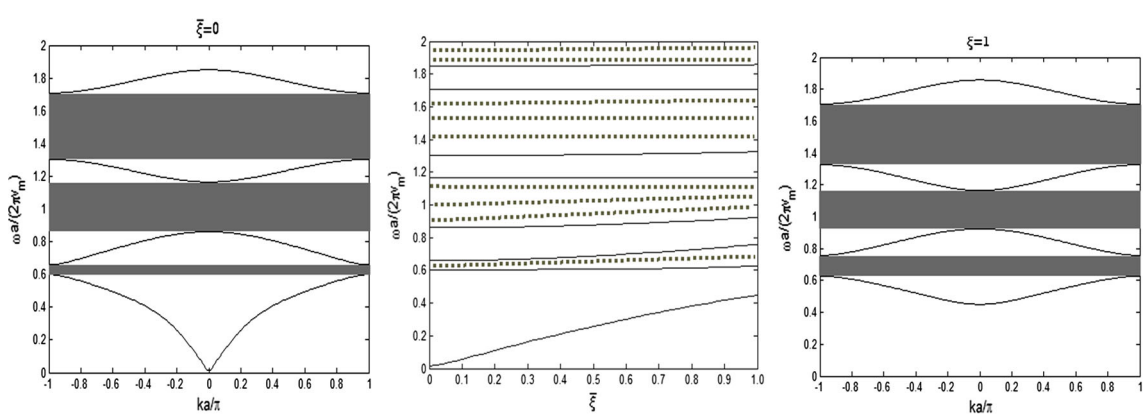

Fig. 3 The dispersive curves and band gaps of anti-plane Bloch waves in the periodic structure consisting of the gradient elastic solids ($\bar{c}_1 = 0.5$, $\bar{c} = 0.77$, $\bar{d}_1 = 0.5$, $\bar{d} = 2$). *Left* in the normal propagation situation ($\bar{\xi} = 0$); *right* in the oblique propagation situation ($\bar{\xi} \neq 0$); *middle* the change of upper and lower band edge

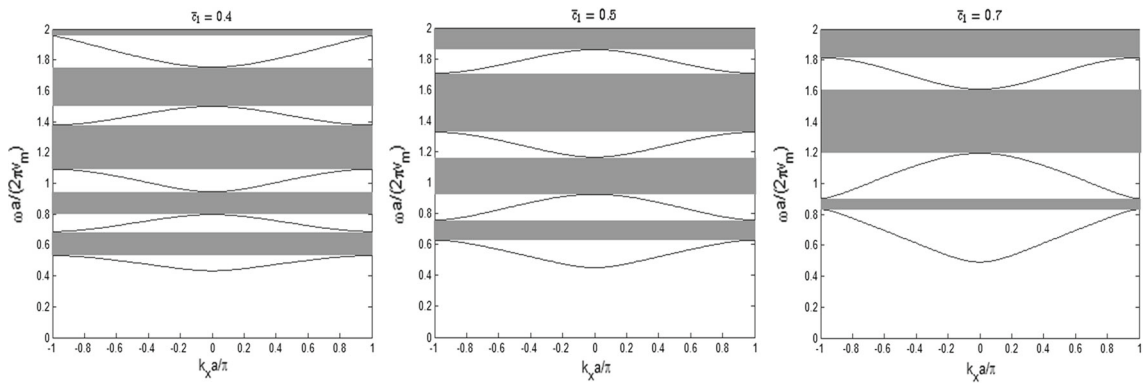

Fig. 4 The influences of the microstructure constant $\bar{c}_1$ on dispersive curves and band gaps of anti-plane Bloch waves ($\bar{c} = 0.77, \bar{d} = 2, \bar{d}_1 = 0.5, \bar{\xi} = 1$)

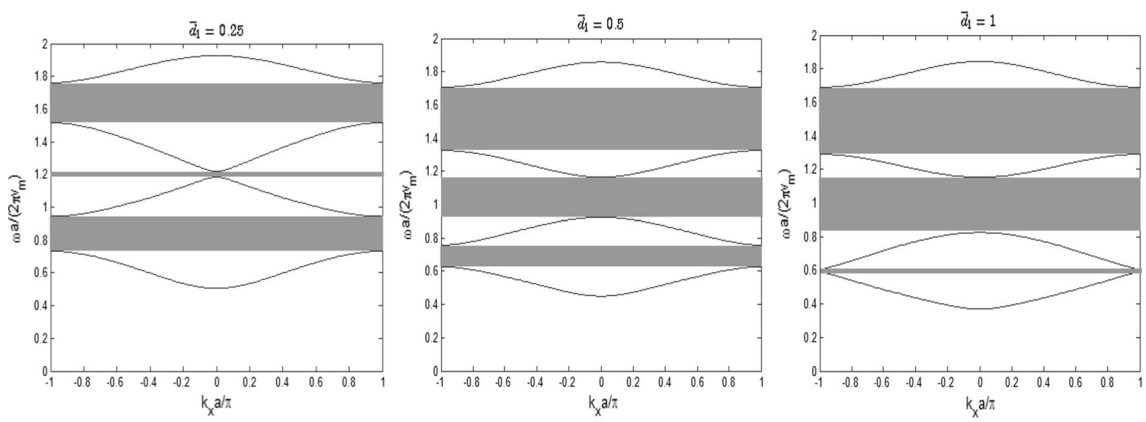

Fig. 5 The influences of the microstructure constant $\bar{d}_1$ on the dispersive curves and the band gaps of anti-plane Bloch waves ($\bar{c}_1 = 0.5, \bar{c} = 0.77, \bar{d} = 2, \bar{\xi} = 1$)

those at the high-frequency range. As a result, the first and second band gaps become narrow. The influences of the apparent wavenumber ξ are also shown in Figs. 2 and 3. Regardless of the gradient elastic solids or the classic elastic solids, the dispersive curves shift toward the high-frequency range as the apparent wavenumber ξ increases and the dispersive curves at low-frequency range shift more evident than those in the high-frequency range. Therefore, the increase in the apparent wavenumber ξ, in general, makes the low-frequency band gaps narrower.

Figures 4 and 5 show the influences of microstructure constant $\bar{c}_1(=\sqrt{c_1}/a)$ and $\bar{d}_1 = d_1/a$ in the gradient elastic solid on the dispersive curves and the band gaps. It is observed that the dispersive curves shift toward the high-frequency range with the increase in microstructure constant $\bar{c}_1$, while the dispersive curves shift toward the low-frequency range with the increase in microstructure constant $\bar{d}_1$. The microstructure constant c_1 is related to the strain gradient effects, and the microstructure constant d_1 is related to the micro-inertia. The two microstructure constants reflect different aspects of the microstructure. It is understandable why the two microstructure constants have different influences on the dispersive curves. It is also noted that the dispersive curves have more evident change near $\bar{\xi} = \xi a = 1$ than near $\bar{\xi} = \xi a = 0$. This means the microstructure effects are more evident for the Bloch wave with shorter wavelength than for the Bloch waves with longer wavelength.

It is well known that the larger contrast of the elastic constants of two solids in a typical single cell of periodic structure is important for the appearance of band gaps. So, it is interesting how the microstructure constant ratio of two gradient elastic solids influences the dispersive curves and the band gaps. Figures 6 and 7 are given to show the influences of the microstructure constant ratio of two gradient elastic solids. It is observed that the dispersive curves shift toward high-frequency range when $\bar{c}(=c_1/c_2)$ increases while the dispersive curves shift toward low-frequency range when $\bar{d}(=d_1/d_2)$ increases. Concomitant with the change of the dispersive curves, the band gaps may become wide or narrow.

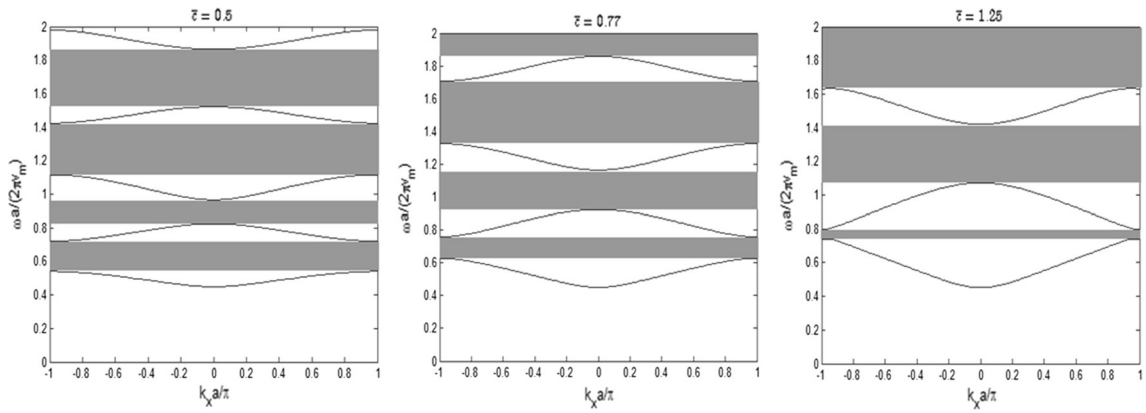

Fig. 6 The influences of the microstructure constant ratio $\bar{c}$ on the dispersive curves and the band gaps of anti-plane Bloch waves ($\bar{c}_1 = 0.5, \bar{d}_1 = 0.5, \bar{d} = 2, \bar{\xi} = 1$)

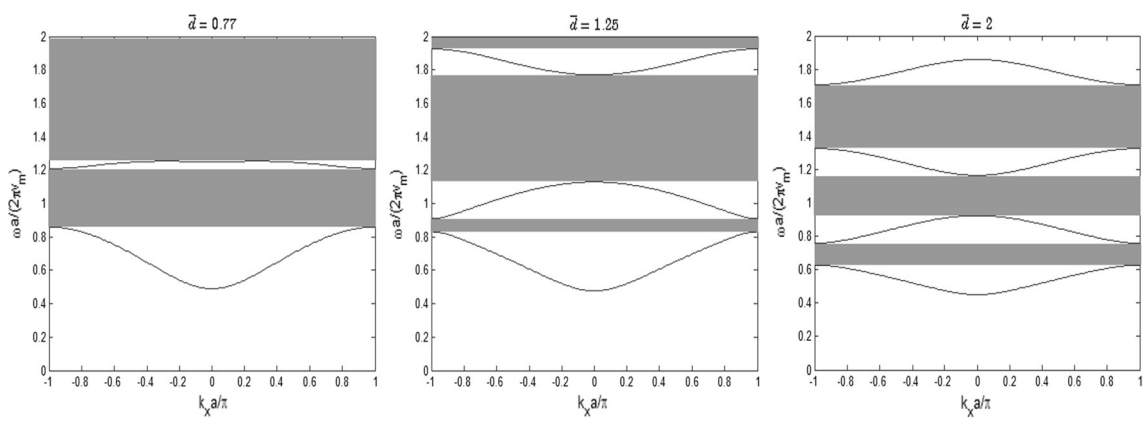

Fig. 7 The influences of the microstructure constant ratio $\bar{d}$ on the dispersive curves and the band gaps of anti-plane Bloch waves ($\bar{c}_1 = 0.5, \bar{c} = 0.77, \bar{d}_1 = 0.5, \bar{\xi} = 1$)

6.2 In-plane Bloch wave

In the normal propagation situation, the Bloch P wave is uncoupled with the Bloch SV wave. Figure 8 shows the dispersive curves of an in-plane Bloch wave in the normal propagation situation. It is observed that the dispersive curves in the periodic structure consisting of gradient elastic solids shift toward the high-frequency range when compared with the dispersive curves in the periodic structure consisting of classical elastic solids. The deviation results from the microstructure effects in the gradient elastic solids. There are four kinds of dispersive waves, i.e., the dispersive P wave and SV wave and two dispersive surface waves. However, there are only two non-dispersive bulk waves, i.e., P wave and SV wave, in the classical elastic solids. It is also noted that the deviation is more evident near $\bar{\xi} = \xi a = 1$ than near $\bar{\xi} = \xi a = 0$. This phenomenon is also noted in the anti-plane propagation situation and can be explained by that the microstructure effects are more evident for a Bloch wave with short wavelength than for a Bloch wave with long wavelength.

Figures 9 and 10 show the dispersive curves of in-plane Bloch waves in the normal propagation situation and in the oblique propagation situation. Regardless of the normal propagation or the oblique propagation, the dispersive curves of Bloch waves in the periodic structure consisting of the gradient elastic solids shift toward the high-frequency range when compared with that in the periodic structure consisting of the classical elastic solids. This means that the microstructure effects exist in both normal propagation situation and the oblique propagation situation and have the same influences in both oblique propagation and normal propagation. As in the anti-plane Bloch wave, the dispersive curves at low-frequency range shift more evident than those at the high-frequency range. Besides, the dispersive curves shift toward the high-frequency range as the apparent wavenumber ξ increases, and the dispersive curves at low-frequency range shift more evident than those in the

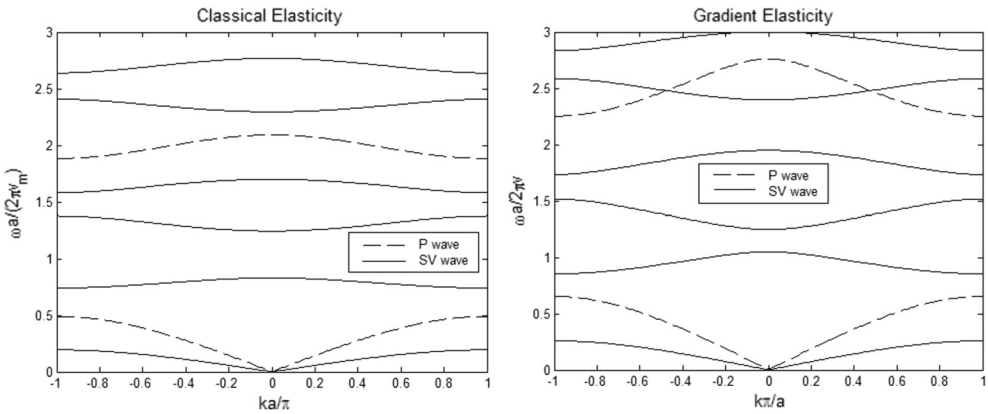

Fig. 8 The dispersive curves of an in-plane Bloch wave in normal propagation situation **a** for the periodic structure consisting of classical elastic solids; **b** for the periodic structure consisting of gradient elastic solids ($\bar{c}_1 = 0.15, \bar{d}_1 = 0.25, \bar{c} = 0.77, \bar{d} = 0.77$)

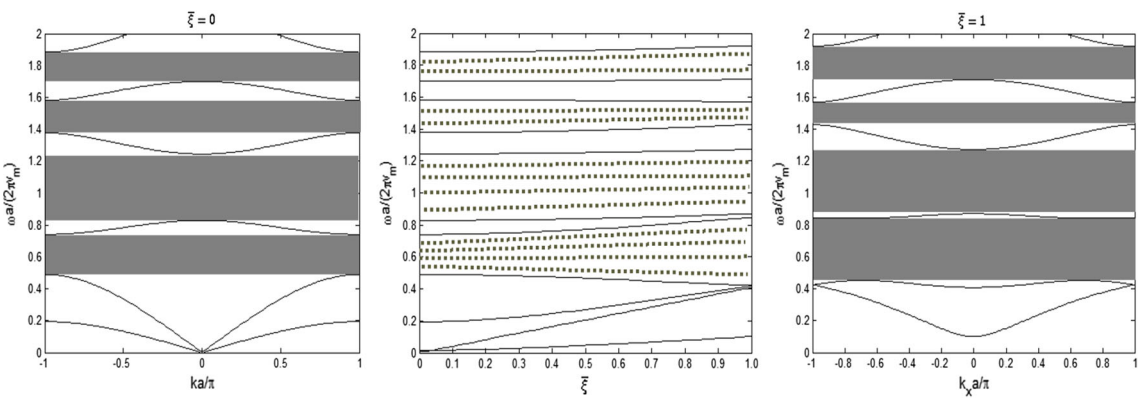

Fig. 9 The dispersive curves and band gaps of in-plane Bloch waves in the periodic structure consisting of the classical elastic solids. *Left* in the normal propagation situation ($\bar{\xi} = 0$); *right* in the oblique propagation situation ($\bar{\xi} \neq 0$); *middle* the change of upper and lower band edge

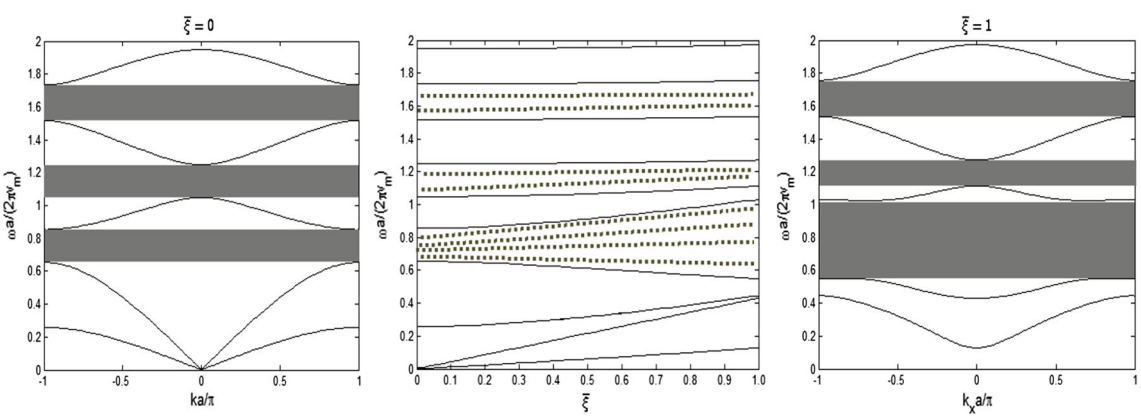

Fig. 10 The dispersive curves and band gaps of in-plane Bloch waves in the periodic structure consisting of the gradient elastic solids ($\bar{c}_1 = 0.15, \bar{d}_1 = 0.25, \bar{c} = 0.77, \bar{d} = 0.77$). *Left* in the normal propagation situation ($\bar{\xi} = 0$); *right* in the oblique propagation situation ($\bar{\xi} \neq 0$); *middle* the change of upper and lower band edge

high-frequency range, regardless of the periodical laminated structure consisting of the classical elastic solids or the gradient elastic solids.

In order to show the influences of two microstructure constants, Figs. 11 and 12 are presented. It is observed that the dispersive curves shift toward the high-frequency range as the microstructure constant c_1

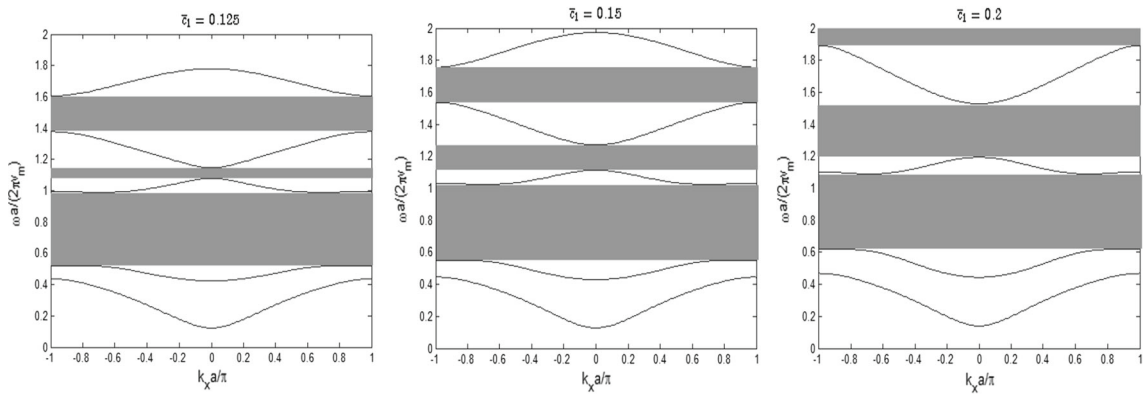

Fig. 11 The influences of the microstructure constant $\bar{c}_1$ on the dispersive curves and the band gaps of in-plane Bloch waves ($\bar{c} = 0.77, \bar{d} = 0.77, \bar{d}_1 = 0.25, \bar{\xi} = 1$)

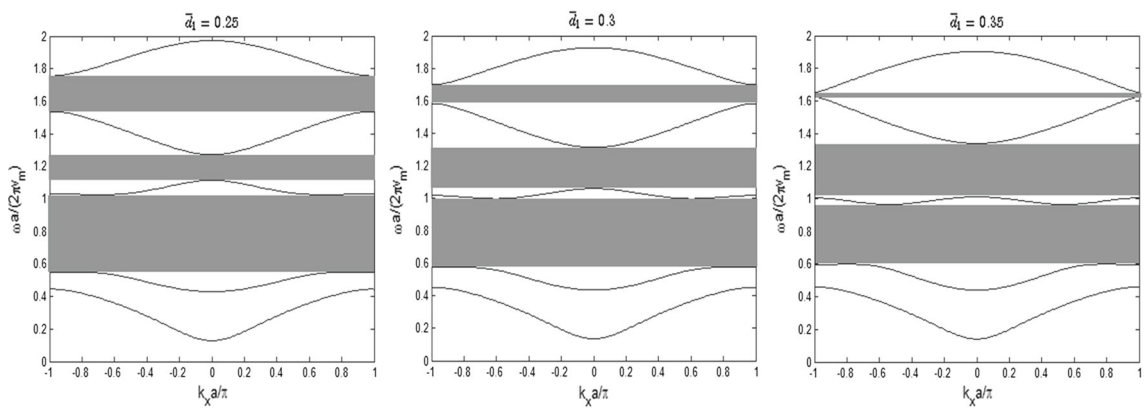

Fig. 12 The influences of the microstructure constant $\bar{d}_1$ on the dispersive curves and the band gaps of in-plane Bloch waves ($\bar{c}_1 = 0.15, \bar{c} = 0.77, \bar{d} = 0.77, \bar{\xi} = 1$)

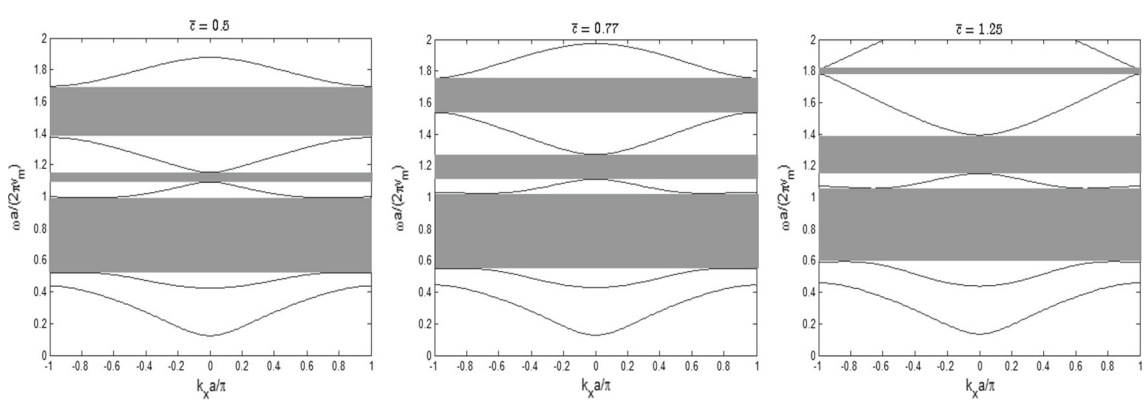

Fig. 13 The influences of the microstructure constant ratio $\bar{c}$ on the dispersive curves and the band gaps of in-plane Bloch waves ($\bar{c}_1 = 0.15, \bar{d} = 0.77, \bar{d}_1 = 0.25, \bar{\xi} = 1$)

increases while the dispersive curves shift toward the low-frequency range as the microstructure constant d_1 increases. However, two microstructure constants, c_1 and d_1, have more evident influences on the dispersive curves at high-frequency range than on those at low-frequency range. A similar phenomenon is observed in the anti-plane Bloch wave situation. The influences of microstructure constant ratio of two gradient elastic solids are also studied and shown in Figs. 13 and 14. Similar with the anti-plane Bloch wave situation, the increase of $\bar{c}(=c_1/c_2)$ makes the dispersive curves shifting toward the high-frequency range while the increase

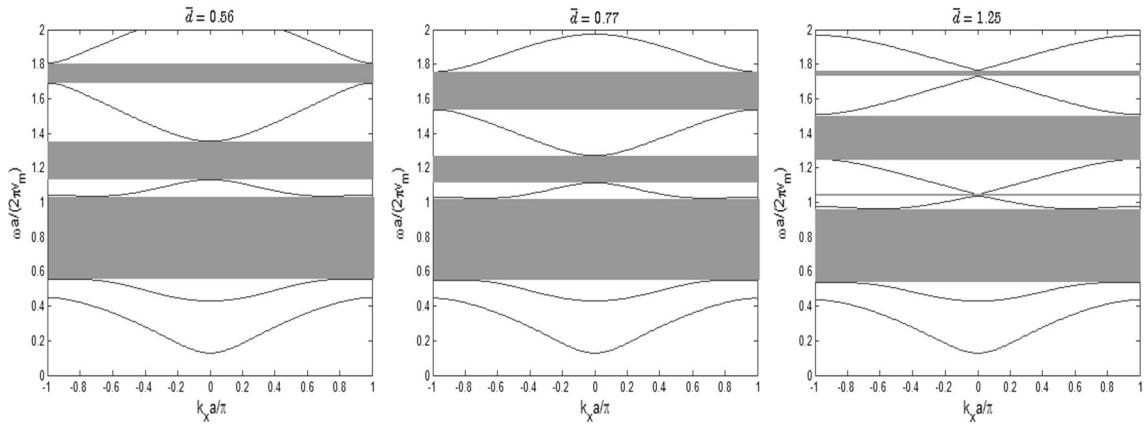

Fig. 14 The influences of the microstructure constant ratio $\bar{d}$ on the dispersive curves and the band gaps of in-plane Bloch waves ($\bar{c}_1 = 0.15, \bar{c} = 0.77, \bar{d}_1 = 0.25, \bar{\xi} = 1$)

of $\bar{d}(=d_1/d_2)$ makes the dispersive shifting toward low-frequency range. But the dispersive curves at the high-frequency range shift more evident than those at the low-frequency range.

7 Conclusions

The dispersive relations of Bloch waves in the one-dimensional periodical laminated structure consisting of two gradient elastic solids which are repeated periodically are studied in the present work. Compared with the classical elastic solid, the gradient elastic solid includes the microstructure effects. With the development of micro- and nano-phononic crystal, the influences of microstructure effects on the propagation behavior of elastic waves with short wavelength become more and more important. It is our main concern in the present work that there are the influences of two microstructure constants, c_1 and d_1, in the gradient elastic solid. The dispersive curves are obtained by solving the dispersive equation numerically. The anti-plane Bloch wave and the in-plane Bloch wave are both considered. Based on these numerical results, the following conclusions can be drawn.

(i) There are three dispersive bulk waves and three dispersive surface waves in the gradient elastic solids. These wave modes make the in-plane and anti-plane Bloch waves in the periodical laminated structure consisting of gradient elastic solids exhibiting evident different dispersive curves from those in the periodical laminated structure consisting of classical elastic solids. Accordingly, the width and central frequency of band gaps have evident deviation.

(ii) There are two microstructure constants, c_1 and d_1, in the present gradient elastic model. c_1 is related to the micro-strain gradient and $d_1$is related to the micro-inertia. Two microstructure constants have opposite influences on the dispersive curves, namely the dispersive curves shifting toward the high-frequency range with the increase of c_1 while shifting toward low-frequency range with the increase of d_1.

(iii) The microstructure effects have more strong influences on the dispersive curves at the high-frequency range than those at low-frequency range. Moreover, Bloch waves with short wavelength are more sensitive to the microstructure effects than the Bloch waves with long wavelength.

(iv) In the oblique propagation situation, in-plane Bloch waves result from the interference between the dispersive P wave and the dispersive SV wave. In the normal propagation situation, the in-plane Bloch waves get decoupled and degrade to the Bloch P wave and Bloch SV wave. Regardless of the oblique propagation or the normal propagation, the dispersive curves of Bloch waves are influenced by the microstructure effects.

(v) The anti-plane Bloch waves result from the interferences of dispersive SH waves, which are different from the in-plane Bloch waves, even though the microstructure effects have similar influences on the anti-plane Bloch waves as on the in-plane Bloch waves. Moreover, the microstructure constants ratio, c_1/c_2 and d_1/d_2, of two gradient elastic solids in a typical single cell of periodical structure have also evident influences on the dispersive curves, but their influences are opposite, regardless of anti-plane Bloch waves or in-plane Bloch waves.

Acknowledgments The work was supported by the National Natural Science Foundation of China (No.10972029) and Opening Fund of State Key Laboratory of Nonlinear Mechanics (LNM).

Appendix 1

In the anti-plane Bloch wave situation, the transfer matrix is $T_j = \left[1/\left(\sigma_{sj}^2 + \tau_{sj}^2\right)\right]\left(t_{kn}^{(j)}\right)_{4\times 4}$ ($j(=A, B)$ indicates layer A or layer B), where

$$
\begin{aligned}
&t_{k1}^{(j)} = e_{k1}^{(j)}\left(\sigma_{sj}^2 + \tau_{sj}^2 - \beta_{sj}^2\right) + \beta_{sj}^2 e_{k2}^{(j)},\\
&t_{k2}^{(j)} = \left[\left(\tau_{sj}^2 - \xi^2\right) - \left(1 - m_{sj}\right)/c_j\right] e_{k3}^{(j)} + \left[\left(1 - m_{sj}\right)/c_j + \left(\sigma_{sj}^2 + \xi^2\right)\right] e_{k4}^{(j)},\\
&t_{k3}^{(j)} = \frac{e_{k3}^{(j)} - e_{k4}^{(j)}}{\mu_j c_j}, \quad t_{k4}^{(j)} = \frac{e_{k2}^{(j)} - e_{k1}^{(j)}}{\mu_j c_j}, k = 1, 2, 3, 4,\\
&e_{11}^{(j)} = \cos\left(\beta_{sj} a_j\right), \quad e_{12}^{(j)} = \cosh\left(\gamma_{sj} a_j\right), \quad e_{13}^{(j)} = \sin\left(\beta_{sj} a_j\right)/\beta_{sj}, \quad e_{14}^{(j)} = \sinh\left(\gamma_{sj} a_j\right)/\gamma_{sj},\\
&e_{21}^{(j)} = -\beta_{sj}\sin\left(\beta_{sj} a_j\right), \quad e_{22}^{(j)} = \gamma_{sj}\sinh\left(\gamma_{sj} a_j\right), \quad e_{23}^{(j)} = \cos\left(\beta_{sj} a_j\right), \quad e_{24}^{(j)} = \cosh\left(\gamma_{sj} a_j\right),\\
&e_{31}^{(j)} = \mu_j\left[-\beta_{sj}\left(1 - m_{sj}\right)\sin\left(\beta_{sj} a_j\right) - c_j\beta_{sj}\left(\sigma_{sj}^2 + \xi^2\right)\sin\left(\beta_{sj} a_j\right)\right],\\
&e_{32}^{(j)} = \mu_j\left[\gamma_{sj}\left(1 - m_{sj}\right)\sinh\left(\gamma_{sj} a_j\right) - c_j\gamma_{sj}\left(\tau_{sj}^2 - \xi^2\right)\sinh\left(\gamma_{sj} a_j\right)\right],\\
&e_{33}^{(j)} = \mu_j\left[\left(1 - m_{sj}\right)\cos\left(\beta_{sj} a_j\right) + c_j\left(\sigma_{sj}^2 + \xi^2\right)\cos\left(\beta_{sj} a_j\right)\right],\\
&e_{34}^{(j)} = \mu_j\left[\left(1 - m_{sj}\right)\cosh\left(\gamma_{sj} a_j\right) - c_j\left(\tau_{sj}^2 - \xi^2\right)\cosh\left(\gamma_{sj} a_j\right)\right],\\
&e_{41}^{(j)} = -\mu_j c_j\beta_{sj}^2\cos\left(\beta_{sj} a_j\right), \quad e_{42}^{(j)} = \mu_j c_j\gamma_{sj}^2\cosh\left(\gamma_{sj} a_j\right),\\
&e_{43}^{(j)} = -\mu_j c_j\beta_{sj}\sin\left(\beta_{sj} a_j\right), \quad e_{44}^{(j)} = \mu_j c_j\gamma_{sj}\sinh\left(\gamma_{sj} a_j\right).
\end{aligned}
$$

Appendix 2

In the in-plane Bloch wave situation, the transfer matrix $T_j = \left(t_{kn}^{(j)}\right)_{4\times 4}$ ($j(=A, B)$ indicates layer A or layer B) is

$$
\begin{aligned}
&t_{k5}^{(j)} = \frac{\left(i\xi e_{k7}^{(j)} - e_{k5}^{(j)}\right) - \left(e_{k6}^{(j)} - e_{k5}^{(j)}\right)\sigma_{pj}^2\Big/\left(\sigma_{pj}^2 + \tau_{pj}^2\right) + i\xi\left(e_{k8}^{(j)} - e_{k7}^{(j)}\right)\sigma_{sj}^2\Big/\left(\sigma_{sj}^2 + \tau_{sj}^2\right)}{\left(\lambda_j + 2\mu_j\right)c_j\sigma_{pj}^2\tau_{pj}^2},\\
&t_{k8}^{(j)} = \frac{e_{k8}^{(j)} - e_{k7}^{(j)}}{\mu_j c_j\left(\sigma_{sj}^2 + \tau_{sj}^2\right)} - t_{k5}^{(j)} i\xi,\\
&t_{k3}^{(j)} = \frac{e_{k6}^{(j)} - e_{k5}^{(j)}}{\sigma_{pj}^2 + \tau_{pj}^2} - t_{k5}^{(j)}\left[\left(\lambda_j + 2\mu_j\right) - \mu_j m_{sj} + \left(\lambda_j + 2\mu_j\right)c_j\left(\sigma_{pj}^2 - \tau_{pj}^2\right)\right] - t_{k8}^{(j)} 2\mu_j c_j i\xi,\\
&t_{k2}^{(j)} = e_{k7}^{(j)} + i\xi t_{k3}^{(j)} + t_{k5}^{(j)}\mu_j i\xi\left[2 - m_{sj} + c_j\left(\sigma_{sj}^2 + 2\xi^2\right)\right] + t_{k8}^{(j)}\mu_j c_j\left(\sigma_{sj}^2 - 2\xi^2\right),\\
&t_{k6}^{(j)} = \frac{\left(e_{k3}^{(j)} - i\xi e_{k1}^{(j)}\right) - \left(e_{k3}^{(j)} - e_{k4}^{(j)}\right)\sigma_{sj}^2\Big/\left(\sigma_{sj}^2 + \tau_{sj}^2\right) + i\xi\left(e_{k1}^{(j)} - e_{k2}^{(j)}\right)\sigma_{pj}^2\Big/\left(\sigma_{pj}^2 + \tau_{pj}^2\right)}{\mu_j c_j\sigma_{sj}^2\tau_{sj}^2},\\
&t_{k7}^{(j)} = t_{k6}^{(j)} i\xi - \frac{e_{k1}^{(j)} - e_{k2}^{(j)}}{\left(\lambda_j + 2\mu_j\right)c_j\left(\sigma_{pj}^2 + \tau_{pj}^2\right)},
\end{aligned}
$$

$$t_{k4}^{(j)} = \frac{e_{k3}^{(j)} - e_{k4}^{(j)}}{\sigma_{sj}^2 + \tau_{sj}^2} - t_{k6}^{(j)} \mu_j \left[1 - m_{sj} + c_j \left(\sigma_{sj}^2 - \tau_{sj}^2\right)\right] + t_{k7}^{(j)} 2\mu_j c_j i\xi,$$

$$t_{k1}^{(j)} = e_{k1}^{(j)} - i\xi t_{k4}^{(j)} + t_{k7}^{(j)} c_j \left(\lambda_j \sigma_{pj}^2 + 2\mu_j \beta_{pj}^2\right)$$
$$- t_{k6}^{(j)} i\xi \left\{\left(2 - m_{sj}\right)\mu_j + c_j \left[\left(\lambda_j + 2\mu_j\right)\sigma_{pj}^2 + 2\mu_j \xi^2\right]\right\}, \quad k = 1, 2, \ldots, 8$$

where

$$e_{11}^{(j)} = \cos\left(\beta_{pj} a_j\right), \quad e_{12}^{(j)} = \cosh\left(\gamma_{pj} a_j\right), \quad e_{13}^{(j)} = i\xi \cos\left(\beta_{sj} a_j\right), \quad e_{14}^{(j)} = i\xi \cosh\left(\gamma_{sj} a_j\right),$$
$$e_{15}^{(j)} = -\beta_{pj} \sin\left(\beta_{pj} a_j\right), \quad e_{16}^{(j)} = \gamma_{pj} \sinh\left(\gamma_{pj} a_j\right), \quad e_{17}^{(j)} = -i\xi \sin\left(\beta_{sj} a_j\right) \Big/ \beta_{sj},$$
$$e_{18}^{(j)} = -i\xi \sinh\left(\gamma_{sj} a_j\right) \Big/ \gamma_{sj}, \quad e_{21}^{(j)} = i\xi \sin\left(\beta_{pj} a_j\right) \Big/ \beta_{pj}, \quad e_{22}^{(j)} = i\xi \sinh\left(\gamma_{pj} a_j\right) \Big/ \gamma_{pj},$$
$$e_{23}^{(j)} = \beta_{sj} \sin\left(\beta_{sj} a_j\right), \quad e_{24}^{(j)} = -\gamma_{sj} \sinh\left(\gamma_{sj} a_j\right), \quad e_{25}^{(j)} = i\xi \cos\left(\beta_{pj} a_j\right),$$
$$e_{26}^{(j)} = i\xi \cosh\left(\gamma_{pj} a_j\right), \quad e_{27}^{(j)} = \cos\left(\beta_{sj} a_j\right), \quad e_{28}^{(j)} = \cosh\left(\gamma_{sj} a_j\right),$$
$$e_{31}^{(j)} = -\beta_{pj} \sin\left(\beta_{pj} a_j\right), \quad e_{32}^{(j)} = \gamma_{pj} \sinh\left(\gamma_{pj} a_j\right), \quad e_{33}^{(j)} = -i\xi\beta_{sj} \sin\left(\beta_{sj} a_j\right),$$
$$e_{34}^{(j)} = i\xi\gamma_{sj} \sinh\left(\gamma_{sj} a_j\right), \quad e_{35}^{(j)} = -\beta_{pj}^2 \cos\left(\beta_{pj} a_j\right), \quad e_{36}^{(j)} = \gamma_{pj}^2 \cosh\left(\gamma_{pj} a_j\right),$$
$$e_{37}^{(j)} = -i\xi \cos\left(\beta_{sj} a_j\right), \quad e_{38}^{(j)} = -i\xi \cosh\left(\gamma_{sj} a_j\right), \quad e_{41}^{(j)} = i\xi \cos\left(\beta_{pj} a_j\right), \quad e_{42}^{(j)} = i\xi \cosh\left(\gamma_{pj} a_j\right),$$
$$e_{43}^{(j)} = \beta_{sj}^2 \cos\left(\beta_{sj} a_j\right), \quad e_{44}^{(j)} = -\gamma_{sj}^2 \cosh\left(\gamma_{sj} a_j\right), \quad e_{45}^{(j)} = -i\xi\beta_{pj} \sin\left(\beta_{pj} a_j\right),$$
$$e_{46}^{(j)} = i\xi\gamma_{pj} \sinh\left(\gamma_{pj} a_j\right), \quad e_{47}^{(j)} = -\beta_{sj} \sin\left(\beta_{sj} a_j\right), \quad e_{48}^{(j)} = \gamma_{sj} \sinh\left(\gamma_{sj} a_j\right),$$
$$e_{51}^{(j)} = \left\{\left(-\lambda_j \sigma_{pj}^2 - 2\mu_j \beta_{pj}^2\right) + \mu_j m_{sj} \beta_{pj}^2 - c_j \left[\lambda_j \sigma_{pj}^4 + 2\mu_j \left(\sigma_{pj}^4 - \xi^4\right)\right]\right\} \sin\left(\beta_{pj} a_j\right) \Big/ \beta_{pj},$$
$$e_{52}^{(j)} = \left\{\left(\lambda_j \tau_{pj}^2 + 2\mu_j \gamma_{pj}^2\right) - \mu_j m_{sj} \gamma_{pj}^2 - c_j \left[\lambda_j \tau_{pj}^4 + 2\mu_j \left(\tau_{pj}^4 - \xi^4\right)\right]\right\} \sinh\left(\gamma_{pj} a_j\right) \Big/ \gamma_{pj},$$
$$e_{53}^{(j)} = \mu_j \left[-2 + m_{sj} - c_j \left(\sigma_{sj}^2 + 2\xi^2\right)\right] i\xi\beta_{sj} \sin\left(\beta_{sj} a_j\right),$$
$$e_{54}^{(j)} = \mu_j \left[2 - m_{sj} + c_j \left(-\tau_{sj}^2 + 2\xi^2\right)\right] i\xi\gamma_{sj} \sinh\left(\gamma_{sj} a_j\right),$$
$$e_{55}^{(j)} = \left\{\left(-\lambda_j \sigma_{pj}^2 - 2\mu_j \beta_{pj}^2\right) + \mu_j m_{sj} \beta_{pj}^2 - c_j \left[\lambda_j \sigma_{pj}^4 + 2\mu_j \left(\sigma_{pj}^4 - \xi^4\right)\right]\right\} \cos\left(\beta_{pj} a_j\right),$$
$$e_{56}^{(j)} = \left\{\left(\lambda_j \tau_{pj}^2 + 2\mu_j \gamma_{pj}^2\right) - \mu_j m_{sj} \gamma_{pj}^2 - c_j \left[\lambda_j \tau_{pj}^4 + 2\mu_j \left(\tau_{pj}^4 - \xi^4\right)\right]\right\} \cosh\left(\gamma_{pj} a_j\right),$$
$$e_{57}^{(j)} = -\mu_j \left[2 - m_{sj} + c_j \left(\sigma_{sj}^2 + 2\xi^2\right)\right] i\xi \cos\left(\beta_{sj} a_j\right),$$
$$e_{58}^{(j)} = -\mu_j \left[2 - m_{sj} + c_j \left(-\tau_{sj}^2 + 2\xi^2\right)\right] i\xi \cosh\left(\gamma_{sj} a_j\right),$$
$$e_{61}^{(j)} = \left\{\left(2 - m_{sj}\right)\mu_j + c_j \left[\left(\lambda_j + 2\mu_j\right)\sigma_{pj}^2 + 2\mu_j \xi^2\right]\right\} i\xi \cos\left(\beta_{pj} a_j\right),$$
$$e_{62}^{(j)} = \left\{\left(2 - m_{sj}\right)\mu_j - c_j \left[\left(\lambda_j + 2\mu_j\right)\tau_{pj}^2 - 2\mu_j \xi^2\right]\right\} i\xi \cosh\left(\gamma_{pj} a_j\right),$$
$$e_{63}^{(j)} = \mu_j \left[\left(\beta_{sj}^2 - \xi^2\right) - m_{sj} \beta_{sj}^2 + c_j \left(\sigma_{sj}^4 - 2\xi^4\right)\right] \cos\left(\beta_{sj} a_j\right),$$
$$e_{64}^{(j)} = \mu_j \left[-\left(\xi^2 + \gamma_{sj}^2\right) + m_{sj} \gamma_{sj}^2 + c_j \left(\tau_{sj}^4 - 2\xi^2\right)\right] \cosh\left(\gamma_{sj} a_j\right),$$
$$e_{65}^{(j)} = -\left\{\left(2 - m_{sj}\right)\mu_j + c_j \left[\left(\lambda_j + 2\mu_j\right)\sigma_{pj}^2 + 2\mu_j \xi^2\right]\right\} i\xi\beta_{pj} \sin\left(\beta_{pj} a_j\right),$$
$$e_{66}^{(j)} = \left\{\left(2 - m_{sj}\right)\mu_j - c_j \left[\left(\lambda_j + 2\mu_j\right)\tau_{pj}^2 - 2\mu_j \xi^2\right]\right\} i\xi\gamma_{pj} \sinh\left(\gamma_{pj} a_j\right),$$
$$e_{67}^{(j)} = -\mu_j \left[\left(\beta_{sj}^2 - \xi^2\right) - m_{sj} \beta_{sj}^2 + c_j \left(\sigma_{sj}^4 - 2\xi^4\right)\right] \sin\left(\beta_{sj} a_j\right) \Big/ \beta_{sj},$$

$$
\begin{aligned}
e_{68}^{(j)} &= -\mu_j\left[-\left(\xi^2+\gamma_{sj}^2\right)+m_{sj}\gamma_{sj}^2+c_j\left(\tau_{sj}^4-2\xi^2\right)\right]\sinh\left(\gamma_{sj}a_j\right)\Big/\gamma_{sj},\\
e_{71}^{(j)} &= -c_j\cos\left(\beta_{pj}a_j\right)\left(\lambda_j\sigma_{pj}^2+2\mu_j\beta_{pj}^2\right),\quad e_{72}^{(j)}=c_j\cosh\left(\gamma_{pj}a_j\right)\left(\lambda_j\tau_{pj}^2+2\mu_j\gamma_{pj}^2\right),\\
e_{73}^{(j)} &= -2\mu_j c_j\beta_{sj}^2 i\xi\cos\left(\beta_{sj}a_j\right),\quad e_{74}^{(j)}=2\mu_j c_j\gamma_{sj}^2 i\xi\cosh\left(\gamma_{sj}a_j\right),\\
e_{75}^{(j)} &= c_j\sin\left(\beta_{pj}a_j\right)\left(\lambda_j\sigma_{pj}^2+2\mu_j\beta_{pj}^2\right),\quad e_{76}^{(j)}=c_j\gamma_{pj}\sinh\left(\gamma_{pj}a_j\right)\left(\lambda_j\tau_{pj}^2+2\mu_j\gamma_{pj}^2\right),\\
e_{77}^{(j)} &= 2\mu_j c_j\beta_{sj}i\xi\sin\left(\beta_{sj}a_j\right),\quad e_{78}^{(j)}=-2\mu_j c_j\gamma_{sj}\sinh\left(\gamma_{sj}a_j\right)i\xi,\\
e_{81}^{(j)} &= -2\mu_j c_j\beta_{pj}\sin\left(\beta_{pj}a_j\right)i\xi,\quad e_{82}^{(j)}=2\mu_j c_j\gamma_{pj}\sinh\left(\gamma_{pj}a_j\right)i\xi,\\
e_{83}^{(j)} &= -\mu_j c_j\beta_{sj}\left(\beta_{sj}^2-\xi^2\right)\sin\left(\beta_{sj}a_1\right),\quad e_{84}^{(j)}=-\mu_j c_j\gamma_{sj}\left(\xi^2+\gamma_{sj}^2\right)\sinh\left(\gamma_{sj}a_j\right),\\
e_{85}^{(j)} &= 2\mu_j c_j\beta_{pj}^2 i\xi\cos\left(\beta_{pj}a_j\right),\quad e_{86}^{(j)}=2\mu_j i\xi\gamma_{pj}^2 c_j\cosh\left(\gamma_{pj}a_j\right),\\
e_{87}^{(j)} &= -\mu_j c_j\cos\left(\beta_{sj}a_1\right)\left(\beta_{sj}^2-\xi^2\right),\quad e_{88}^{(j)}=\mu_j c_j\cosh\left(\gamma_{sj}a_j\right)\left(\xi^2+\gamma_{sj}^2\right).
\end{aligned}
$$

Appendix 3

In the normal propagation situation, the transfer matrix $T_j=\left[1/\left(\sigma_{rj}^2+\tau_{rj}^2\right)\right]\left(t_{kn}^{(j)}\right)_{4\times4}$ ($j(=A,B)$ indicates layer A or layer B) of Bloch SH wave, Bloch P wave, and Bloch SV wave is

$$
\begin{aligned}
t_{11}^{(j)} &= \sigma_{rj}^2\cosh\left(\tau_{rj}a_j\right)+\tau_{rj}^2\cos\left(\sigma_{rj}a_j\right),\quad t_{12}^{(j)}=\sigma_{rj}\sin\left(\sigma_{rj}a_j\right)+\tau_{rj}\sinh\left(\tau_{rj}a_j\right),\\
t_{13}^{(j)} &= \left[\tau_{rj}\sin\left(\sigma_{rj}a_j\right)-\sigma_{rj}\sinh\left(\tau_{rj}a_j\right)\right]\Big/c_j\varepsilon_j\sigma_{rj}\tau_{rj},\\
t_{14}^{(j)} &= \left[\cosh\left(\tau_{rj}a_j\right)-\cos\left(\sigma_{rj}a_j\right)\right]\Big/c_j\varepsilon_j,\quad t_{21}^{(j)}=\sigma_{rj}^2\tau_{rj}\sinh\left(\tau_{rj}a_j\right)-\tau_{rj}^2\sigma_{rj}\sin\left(\sigma_{rj}a_j\right),\\
t_{22}^{(j)} &= \sigma_{rj}^2\cos\left(\sigma_{rj}a_j\right)+\tau_{rj}^2\cosh\left(\tau_{rj}a_j\right),\quad t_{23}^{(j)}=\left[\cos\left(\sigma_{rj}a_j\right)-\cosh\left(\tau_{rj}a_j\right)\right]\Big/c_j\varepsilon_j,\\
t_{24}^{(j)} &= \left[\tau_{rj}\sinh\left(\tau_{rj}a_j\right)+\sigma_{rj}\sin\left(\sigma_{rj}a_j\right)\right]\Big/c_j\varepsilon_j,\\
t_{31}^{(j)} &= -c_j\varepsilon_j\sigma_{rj}\tau_{rj}\left[\sigma_{rj}^3\sinh\left(\tau_{rj}a_j\right)+\tau_{rj}^3\sin\left(\sigma_{rj}a_j\right)\right],\\
t_{32}^{(j)} &= c_j\varepsilon_j\sigma_{rj}^2\tau_{rj}^2\left[\cos\left(\sigma_{rj}a_j\right)-\cosh\left(\tau_{rj}a_j\right)\right],t_{33}^{(j)}=\tau_{rj}^2\cos\left(\sigma_{rj}a_j\right)+\sigma_{rj}^2\cosh\left(\tau_{rj}a_j\right),\\
t_{34}^{(j)} &= \tau_{rj}\sigma_{rj}\left[\tau_{rj}\sin\left(\sigma_{rj}a_j\right)-\sigma_{rj}\sinh\left(\tau_{rj}a_j\right)\right],\\
t_{41}^{(j)} &= c_j\varepsilon_j\sigma_{rj}^2\tau_{rj}^2\left[\cosh\left(\tau_{rj}a_j\right)-\cos\left(\sigma_{rj}a_j\right)\right],\\
t_{42}^{(j)} &= c_j\varepsilon_j\left[\tau_{rj}^3\sinh\left(\tau_{rj}a_j\right)-\sigma_{rj}^3\sin\left(\sigma_{rj}a_j\right)\right],\\
t_{43}^{(j)} &= -\tau_{rj}\sinh\left(\tau_{rj}a_j\right)-\sigma_{rj}\sin\left(\sigma_{rj}a_j\right),\quad t_{44}^{(j)}=\tau_{rj}^2\cosh\left(\tau_{rj}a_j\right)+\sigma_{rj}^2\cos\left(\sigma_{rj}a_j\right).
\end{aligned}
$$

$r=s$ denotes Bloch SH wave and Bloch SV wave, and $r=p$ denotes Bloch P wave. $\varepsilon=\mu$ for Bloch SH wave and Bloch SV wave, and $\varepsilon=\lambda+2\mu$ for Bloch P wave.

References

1. Chen, G., Narayanaswamy, A., Dames, C.: Engineering nanoscale phonon and photon transport for direct energy conversion. Superlattice Microstruct. **35**, 161–172 (2004)
2. Cai, B., Wei, P.J.: Influences of gradient profile on the band gap of two-dimensional phononic crystal. J. Appl. Phys. **110**, 103514 (2011)
3. Cai, B., Wei, P.J.: Surface/interface effects on dispersion relations of 2D phononic crystals with parallel nanoholes or nanofibers. Acta Mech. **224**, 2749–2758 (2013)
4. Eringen, A.C.: Mechanics of micromorphic materials. In: Görtler, H. Proceedings of XI. International Congress of Applied Mechanics, Springer, New York (1964)
5. Eringen, A.C.: Linear theory of micropolar elasticity. J. Math. Mech. **15**, 909–924 (1966)

6. Eringen, A.C.: Theory of thermo-microstretch elastic solids. Int. J. Eng. Sci. **28**, 1291–1301 (1990)
7. Eringen, A.C.: Nonlocal Continuum Field Theories. Springer, Berlin (2001)
8. Green, A.E., Rivlin, R.S.: Multipolar continuum mechanics. Arch Ration. Mech. Anal. **17**, 113–147 (1964)
9. Green, A.E.: Micro-materials and multipolar continuum mechanics. Int. J. Eng. Sci. **3**, 533–537 (1965)
10. Georgiadis, H.G.: The Mode III Crack Problem in microstructured solids governed by dipolar gradient elasticity: static and dynamic analysis. ASME J. Appl. Mech. **70**, 517–530 (2003)
11. Georgiadis, H.G., Vardoulakis, I., Velgaki, E.G.: Dispersive Rayleigh-wave propagation in microstructured solids characterized by dipolar gradient elasticity. J. Elast. **74**, 17–45 (2004)
12. Gourgiotis, P.A., Georgiadis, H.G., Neocleous, I.: On the reflection of waves in half-spaces of microstructured materials governed by dipolar gradient elasticity. Wave Motion **50**, 437–455 (2013)
13. Gourgiotis, P.A., Georgiadis, H.G.: Torsional and SH surface waves in an isotropic and homogenous elastic half-space characterized by the Toupin–Mindlin gradient theory. Int. J. Solids Struct. **62**, 217–228 (2015)
14. Håkansson, A., Sánchez-Dehesa, J., Sanchis, L.: Acoustic lens design by genetic algorithms. Phys. Rev. B **70**, 214302 (2004)
15. Hou, Z., Wu, F., Liu, Y.: Phononic crystals containing piezoelectric material. Solid State Commun. **130**, 745–749 (2004)
16. Khelif, A., Choujaa, A., Benchabane, S., Djafari-Rouhani, B., Laude, V.: Guiding and bending of acoustic waves in highly confined phononic crystal waveguides. Appl. Phys. Lett. **84**, 4400–4402 (2004)
17. Kushwaha, M.S., Halevi, P., Dobrzynski, L., Djafari-Rouhani, B.: Acoustic band structure of periodic elastic composites. Phys. Rev. Lett. **71**, 2022–2025 (1993)
18. Liu, Z., Zhang, X., Mao, Y., Zhu, Y.Y., Yang, Z., Chan, C.T. et al.: Locally resonant sonic materials. Science **289**, 1734–1736 (2000)
19. Lan, M., Wei, P.J.: Laminated piezoelectric phononic crystal with imperfect interfaces. J. Appl. Phys. **111**, 013505 (2012)
20. Lan, M., Wei, P.J.: Band gap of piezoelectric/piezomagnetic phononic crystal with graded interlayer. Acta Mech. **225**, 1779–1794 (2014)
21. Li, Y.Q., Wei, P.J.: Reflection and transmission of plane waves at the interface between two different dipolar gradient elastic half-spaces. Int. J. Solids Struct. **56**, 194–208 (2015)
22. Li, Y.Q., Wei, P.J., Tang, Q.H.: Reflection and transmission of elastic waves at the interface between two gradient-elastic solids with surface energy. Eur. J. Mech. A-Solids **52**, 54–71 (2015)
23. Lu, M.H., Feng, L., Chen, Y.F.: Phononic crystals and acoustic metamaterials. Mater. Today **12**, 34–42 (2009)
24. Mindlin, R.D., Tiersten, H.F.: Effects of couple stress in linear elasticity. Arch. Ration. Mech. Anal. **11**, 415–448 (1962)
25. Mindlin, R.D.: Micro-structure in linear elasticity. Arch. Ration. Mech. Anal. **16**, 51–78 (1964)
26. Parfitt, V.R., Eringen, A.C.: Reflection of plane waves from the flat boundary of a micropolar half-space. J. Acoust. Soc. Am. **45**, 1258–1272 (1969)
27. Pang, Y., Jiao, F.Y., Liu, J.X.: Propagation behavior of elastic waves in one-dimensional piezoelectric/piezomagnetic phononic crystal with line defects. Acta Mech. Sinica **30**, 703–713 (2014)
28. Qiu, C., Liu, Z., Shi, J., Chan, C.T.: Directional acoustic source based on the resonant cavity of two-dimensional phononic crystals. Appl. Phys. Lett. **86**, 224105 (2005)
29. Sigalas, M.M., Economou, E.N.: Elastic and acoustic wave band structure. J. Sound Vib. **158**, 377–382 (1992)
30. Sun, J.Z., Wei, P.J.: Band gaps of 2D phononic crystal with imperfect interface. Mech. Adv. Mater. Struct. **21**, 107–116 (2014)
31. Toupin, R.A.: Elastic materials with couple stresses. Arch. Ration. Mech. Anal. **11**, 385–414 (1962)
32. Tomar, S.K., Gogna, M.L.: Reflection and refraction of longitudinal wave at an interface between two micropolar elastic solids at welded contact. J. Acoust. Soc. Am. **97**, 822–830 (1995)
33. Tomar, S.K., Monika, G.: Reflection and transmission of waves from a plane interface between two microstretch solid half-spaces. Int. J. Eng. Sci. **43**, 139–169 (2005)
34. Wang, Y.Z., Li, F.M., Kishimoto, K., Wang, Y.S., Huang, W.H.: Elastic wave band gaps in magnetoelectroelastic phononic crystals. Wave Motion **46**, 47–56 (2009)
35. Wang, Y.Z., Li, F.M., Kishimoto, K., Wang, Y.S., Huang, W.H.: Band gaps of elastic waves in three-dimensional piezoelectric phononic crystals with initial stress. Eur. J. Mech. A-Solids **29**, 182–189 (2010)
36. Yang, S., Page, J., Liu, Z., Cowan, M., Chan, C., Sheng, P.: Focusing of sound in a 3D phononic crystal. Phys. Rev. Lett. **93**, 024301 (2004)
37. Zhao, Y.P., Wei, P.J.: The band gap of 1D viscoelastic phononic crystal. Comp. Mater. Sci. **46**, 603–606 (2009)
38. Zhao, Y.P., Wei, P.J.: The influence of viscosity on band gaps of 2D phononic crystal. Mech. Adv. Mater. Struct. **17**, 383–392 (2010)
39. Zhan, Z.Q., Wei, P.J.: Influences of anisotropy on band gaps of 2D phononic crystal. Acta. Mech. Solida Sin. **23**, 182–188 (2010)
40. Zhan, Z.Q., Wei, P.J.: Band gaps of three-dimensional phononic crystal with anisotropic spheres. Mech. Adv. Mater. Struct. **21**, 245–254 (2014)